www.sciencemag.org/content/342/6160/830/suppl/DC1

Supplementary Materials for

Room-Temperature Quantum Bit Storage Exceeding 39 Minutes Using Ionized Donors in Silicon-28

Kamyar Saeedi, Stephanie Simmons, Jeff Z. Salvail, Phillip Dluhy, Helge Riemann, Nikolai V. Abrosimov, Peter Becker, Hans-Joachim Pohl, John J. L. Morton, Mike L. W. Thewalt*

*Corresponding author. E-mail: thewalt@sfu.ca

Published 15 November 2013, *Science* **342**, 830 (2013)
DOI: 10.1126/science.1239584

This PDF file includes:

Materials and Methods

Samples and sample properties

The results presented here for temperatures ≤4.2 K used the same sample, sample holder, liquid He immersion dewar and electromagnet system as described in our study of the nuclear spin of neutral ^{31}P (*9*), while results involving ramping the sample temperature between 4.2 K and room temperature required a new sample, sample holder and high homogeneity split-pair superconducting magnet system with a Vari-Temp style sample chamber which allows liquid He to be either brought in from or pushed back to a storage reservoir. Both the original 11.8 x 4.5 x 1.7 mm^3 sample and the new 5 x 4.7 x 1.7 mm^3 sample are cut from slice Si28-10Pr11.02.2 taken from the seed end of the Avogadro crystal (*26*), enriched to 99.995% ^{28}Si and containing 46 ppm ^{29}Si, ~5x10^{11} cm^{-3} ^{31}P, 5x10^{13} cm^{-3} boron, <10^{13} cm^{-3} oxygen and <10^{14} cm^{-3} carbon. The samples were etched in HF/HNO_3 to remove any surface damage which could cause strain, and sit loosely in their sample holders, again to avoid any strain which could split and broaden the optical transitions.

Since the concentration of boron acceptors is one hundred times that of the ^{31}P donors, one would expect that in equilibrium at temperatures of 4.2 K and below all of the donors would be ionized, along with an equal number of acceptors, but donor-acceptor-pair recombination in Si is a very slow process at such low concentrations (*15*). Indeed, during the present study we realized that a significant part of the decay of the neutral donor signal seen in our previous study (*9*) in fact resulted from this slow ionization of the D^0. In our initial efforts to study D^+ we observed a slow loss of the ionized donor population at 4.2 K on a similar time scale. We discovered that this was due to photoneutralization from very low levels of above-gap light reaching the sample, which was eliminated by adding a global shutter immediately in front of the dewar window, and taking other measures to suppress background light. After these improvements the loss of D^+ at low temperature became undetectable, as seen in Fig. 3A.

At liquid He temperatures and in the dark there will be no free carriers in the sample, but this changes as the temperature is raised. Above ~30 K the neutral boron begin to thermally ionize (~1% ionized at 30 K) and above 70 K essentially all the boron are ionized, providing ~5x10^{13} cm^{-3} of free holes. This free hole concentration is essentially constant between 70 K and room temperature. Due to the p-type doping, thermally generated e^- do not begin to appear until 230 K (~1 cm^{-3}), increasing to ~1.2x10^6 cm^{-3} at room temperature. These free electrons and holes could in principle have acted to depolarize or decohere the D^+ nuclear spins, but they are seen to have a relatively small effect. At room temperature the probability of an e^- being bound to a D^+ to give a D^0 in the ground state is ~ 2x10^{-13} for our sample doping, which could account for some of the observed decoherence. This small probability of having a D^0 in its ground state at room temperature could be further reduced by going to higher p-type doping, or by using a semiconductor with a wider band gap.

Apparatus

A schematic of the apparatus is shown in Fig. S1, and we begin by describing those components which are common to both the constant cryogenic temperature and temperature ramp experiments, paying particular attention to improvements which have

been made to the apparatus used for the previous (*9*) D^0 measurements. Resonant optical excitation is provided by two single-frequency distributed-feedback Yb-doped fiber lasers followed by Yb-doped fiber amplifiers. For the transient measurements these lasers are tuned to line 4 and line 6 of the D^0X absorption transitions. We have improved the system for the task of D^+ readout by adding a third optical beam tuned to line 5, which is derived from the line 6 laser by downshifting a portion of the beam by 56 MHz (~RF↑) using an acousto-optic modulator (AOM). Above-gap excitation, which is required to generate the free e^- (and holes) needed to photoneutralize the donors during initialization and readout, is provided by a 1047 nm Nd-YLF laser. The four laser beams are turned on and off using fast electromechanical shutters, and a fifth global shutter was added to block any above-gap light from reaching the sample during the NMR manipulations and the temperature ramps. The two Yb-doped fiber lasers are locked and scanned with respect to a stable reference cavity, which is itself locked to a frequency-stabilized HeNe laser, giving a long term laser frequency stability and repeatability of a few MHz.

For the 4.2 K preparation and readout used in the temperature ramp experiments, the excitation intensities at the sample were approximately 90 $mWcm^{-2}$ for the line 6 laser, 7 mW cm^{-2} for the line 4 and line 5 lasers, and 0.02 $mWcm^{-2}$ for the above-gap 1047 nm laser. At temperatures below 4.2 K the optimum 1047 nm laser power and the readout transient times were found to be temperature dependent, which we ascribe to the capture of e^- onto D^0 and free holes onto A^0 to form D^- and A^+ centers, since these centers have the ~2 meV binding energies which would explain strong thermal dissociation at 4.2 K and binding at lower temperatures (*20*). The noncontact photoconductive readout method, which is a form of electrically detected magnetic resonance (EDMR) we have referred to as Auger electron detected magnetic resonance (AEDMR), is essentially unchanged from our previous study of neutral ^{31}P (*9*). At a given preparation/readout temperature the 1047 nm above-gap laser power was adjusted to the minimum needed for efficient photoneutralization, since excess 1047 nm laser power has two deleterious effects. First, by generating more e^- and free holes it 'shorts out' the sample, making the impedance changes from the resonantly created e^- more difficult to observe. Second, by creating free excitons which can bind onto D^0 to form D^0X, the above-gap excitation enables a process which under our low field conditions, where the e^- and donor electrons are essentially unpolarized, drives the nuclear polarization towards equilibrium, counteracting our resonant hyperpolarization (*27*). Capture of the unpolarized e^- generated by the above-gap excitation onto D^+ could also reduce the achievable hyperpolarization.

All experiments were done at the same $B_0 \cong 845.3$ G used in our previous study of $^{31}P^0$ (*9, 16*). This is an advantageous field for studying the nuclear spin of $^{31}P^0$, since at this field $\partial RF\uparrow/\partial B_0 = \partial RF\downarrow/\partial B_0 = 0$, making them clock transitions and greatly relaxing the requirements for B_0 field homogeneity and stability (*16*). There is no such advantage for $^{31}P^+$, since $RF^+ = \gamma_n B_0$, where γ_n is the gyromagnetic ratio for $^{31}P^+$, 17.23 MHz/T (*11*). For experiments at or below 4.2 K the previous electromagnet system was used, with the addition of a more precise NMR gaussmeter to stabilize B_0 instead of the previous Hall Effect gaussmeter. For experiments above 4.2 K, a Vari-Temp style dewar was needed so that liquid He could be moved back and forth between a storage reservoir and the

sample chamber, and this was provided by a high homogeneity split pair superconducting solenoid dewar, operated at $B_0 \cong 845.3$ G in persistent current mode.

The RF pulses at frequencies RF↑ ≅ 55.847 MHz, RF↓ ≅ 61.677 MHz and $RF^+ \cong$ 1.4567 MHz were generated by an NMR synthesizer (Spincore Pulseblaster DDS) locked to an external Rb clock for stability, and amplified to the 10 W level. A multifrequency tuner external to the dewar was used to match the 6 turn RF coil to the 50 Ohm output of the amplifier at both 1.43 MHz and ~59 MHz (half way between RF↑ and RF↓). Since the B_0 field at the sample could not be set precisely, the three resonance frequencies were determined before every experiment by collecting Ramsey fringe scans, and the three π pulse lengths were determined by collecting Rabi oscillation scans. Typical π pulse lengths were 150 to 160 μs for RF↑ and RF↓, and 90 μs for RF^+.

Temperature Ramping

Experiments requiring the initialization of the sample at 4.2 K followed by raising it to room temperature (e.g. for T_2 measurements), and returning it to 4.2 K for readout required the construction of a new sample holder, which is shown in Fig. S2. A small, evacuated glass mini-dewar, which is a snug fit in the Vari-Temp sample chamber tube, surrounds the sample holder so that it could be warmed to room temperature without needing to warm the entire sample tube/window block/RF coil. At the top of the sample holder is a standard Cu heater block, with a bifilar-wound 25 Ohm heater and a rectangular Cu stub pointing downwards. The sample holder itself is made of four strips of sapphire and a strip of high purity natural Si, all 5mm wide, which are glued to each other and to the Cu stub on the heater block using thermally conductive epoxy (Stycast 2850 FT). The sample fits loosely into the compartment formed by the four sapphire strips, sitting on the bottom strip under its own weight, and with ~150 microns between each 5x4.7 mm^2 face and the sapphire. Two temperature sensors are attached to the sapphire using the same thermally conductive epoxy, one at the heater end (sensor1) and one below the sample compartment (sensor2). The two open sides of the sample compartment are covered by brass shim strips which both enclose the sample compartment and also act as electrodes for the capacitive photoconductivity measurement.

The sample and sample holder are immersed in liquid He at 4.2 K for initialization and readout. The first step of a temperature ramp is to pressurize the sample chamber and open the He needle valve, thus pushing the liquid He from the sample chamber back into the He reservoir. After this the needle valve is closed and the sample remains under 1 atmosphere of He gas. A proportional temperature controller set to 298 K and controlled by sensor2 is then turned on, initially providing 25 W to the heater. The sample holder temperature rises very quickly at first due to the low heat capacities at low temperature, but as this slows down an increasing temperature gradient occurs along the length of the sample holder, and sensor1 throttles the heater power so that the temperature at the heater end of the sample holder never rises above 350 K. The temperature difference between sensor1 and sensor2 rises to ~150 K during the temperature up ramp, but decreases as the bottom of the sample holder approaches room temperature and proportional control based on the sensor2 temperature takes over. Two minutes after sensor2 first reaches room temperature the gradient along the sample holder has dropped to ~20 K, and at this point the manipulation of the nuclear spins begins.

Mounting a temperature sensor directly to the sample is not feasible since our optical ensemble measurement is highly sensitive to strain, but we calculate the thermal time constant of the sample coupled to the sample holder through He gas to be seconds at room temperature. Given the positioning of sensor2, the ~6 minute ramp up time, and the 2 minute wait time at room temperature before any measurement, we are confident that the sample is at or slightly above 298 K during measurement.

During cooldown, the heater power is turned off and the needle valve is opened a controlled amount, so that an overpressure on the He reservoir transfers liquid He to the sample chamber slowly enough that the He boiloff gas is used to efficiently cool the sample holder. After ~4 minutes the sample, sample holder and both sensors are immersed under liquid He, at which point the readout process can begin.

Hyperpolarization

In the next three subsections we describe in detail the stages of the experiment shown in Fig. 2A, with reference to the transitions shown in Fig. 1C. Step {1} hyperpolarizes the donor nuclear spins, and is the same process used previously in our study of neutral ^{31}P (*9*). The 500 ms hyperpolarization time is much longer than what is required to obtain a good polarization, but is kept long so as to remove all history of the previous state of the sample. The 1047 nm laser is on to photoneutralize the donors, and the laser on line 6 quickly converts D^0 in state $|\uparrow\Downarrow\rangle$ into D^0X, which Auger ionize to give e^- and D^+ in state $|\Downarrow\rangle$. Electron capture produces either $|\uparrow\Downarrow\rangle$ or $|\downarrow\Downarrow\rangle$, resulting in a buildup of population in $|\downarrow\Downarrow\rangle$. In a similar way, the laser on line 4 moves population from $|\downarrow\Uparrow\rangle$ to $|\uparrow\Uparrow\rangle$, and $RF_\uparrow$ flips the nuclear spin, moving population from $|\uparrow\Uparrow\rangle$ to $|\uparrow\Downarrow\rangle$, where it is quickly ionized by the laser on line 6. At the end of step {1}, almost all of the donors are either in state $|\downarrow\Downarrow\rangle$ or state $|\Downarrow\rangle$. Since there is no laser tuned to ionize $|\downarrow\Downarrow\rangle$, we instead flip $|\Downarrow\rangle$ to $|\Uparrow\rangle$ in step {2}, $|\downarrow\Downarrow\rangle$ to $|\downarrow\Uparrow\rangle$ in step {3}, and then use the laser on line 4 to ionize $|\downarrow\Uparrow\rangle$ to $|\Uparrow\rangle$ in step{4}. By step {5} we estimate that over 90% of the donors are both ionized and polarized into state $|\Uparrow\rangle$, based on our inability to observe any NMR response above the noise level from the other states.

Manipulation

The manipulation section ({6} to{8}) of Fig. 2A shows a simple Hahn echo sequence, where the $+\pi/2$ pulse at step {6} places the system in a coherent superposition with nominal phase X, the π pulse at {7} refocuses any constant dephasing, and the $\pi/2$ pulse at {8} projects the remaining coherence into a $|\Downarrow\rangle$ population. This is repeated with a $-\pi/2$ pulse at {6}, resulting in a $|\Uparrow\rangle$ population after projection at {8}, so that a difference measurement can be made between the readouts generated by the two phase-cycled initial states. For T_1 measurements, the π pulse of the Hahn echo sequence (step {7}) is removed and the two $\pi/2$ pulses (steps {6} and {8}) are placed close together in time, with the evolution of the system occurring after these pulses, between steps {8} and {9}. For the $+\pi/2$ pulse at step {6} this is equivalent to a $+\pi$ pulse, leaving the system in state $|\Downarrow\rangle$ at the end of step {8}, while for the $-\pi/2$ pulse at {6} it is equivalent to no operation, leaving the system in state $|\Uparrow\rangle$ after step {8}, again allowing for a difference measurement after the two readouts. The Ramsey fringe measurement to determine T_2^* is very similar to the T_1 measurement, but the time evolution occurs between the two $\pi/2$

pulses, and the RF frequency is offset from the actual resonance frequency by a known amount in order to produce fringes with a suitable period.

The Hahn echo sequence can only refocus the effects of inhomogeneities which are essentially static, and longer coherence times can be obtained using periodic refocusing, or dynamic decoupling, with a series of π pulses which can eliminate the effects of low frequency noise and drift (*28, 29*). We have shown that a repeated, relatively simple series of $\pm\pi$ rotations around the X and Y axes, known as XY-16 (*19*), is remarkably resistant to degradation due to pulse errors, and can protect an arbitrary coherent initial state against decay (*9*). For all the results shown here the delay between the π pulses in the XY-16 sequence was 8 ms. As the time 2τ between π pulses is reduced, the low frequency B_0 noise is suppressed to an increasing frequency cutoff, but a tradeoff is reached because of the accumulation of pulse errors as the number of pulses grows.

A τ of 4 ms was near optimal for XY-16 decoupling at low temperature and worked well for short delays at room temperature (less than ~10 min.), but for longer times at room temperature a rapid decrease in the nuclear spin coherence signal intensity was observed. We hypothesized that this was due to a slow warming of the RF coil and transmission line for longer room temperature measurements, causing the coil tuning to change and making the π pulse length inaccurate beyond the point which could be corrected for by the XY-16 sequence. We therefore replaced the simple π pulses with BB1 composite π pulses (*30*), which give a closer approximation to an exact π rotation when the π pulse length is incorrect by a factor which is constant over the duration of the composite pulse. The five individual π pulses of each BB1 composite pulse were placed close together in time, with the time evolution of the system taking place during the 8 ms between the composite π pulses. This provided an adequate solution to our inability to match coil parameters as a function of temperature. A better solution would be to operate the RF coil and transmission line at a constant temperature, thermally isolated from the sample holder.

Readout

At a temperature of 4.2 K (or below in the case of the all-cryogenic measurements), the ionized donors are neutralized in step {10}, but the neutralizing electrons have negligible polarization, so for example $|\Uparrow\rangle$ polarized D^+ would result in equal $|\downarrow\Uparrow\rangle$ and $|\uparrow\Uparrow\rangle$ populations. Our original readout scheme (*9*) for studying D^0 was optimized for measuring the population of a single hyperfine state, and therefore only reads out half the polarized D^+ after neutralization. The previous readout scheme also suffers from strong transients, as seen in Fig. 2B, since the readout laser on line 4 moves population from $|\downarrow\Uparrow\rangle$ to $|\uparrow\Uparrow\rangle$ during step {11}, and again after the single π pulse at RF$\downarrow$ (step {12}), moves population from $|\downarrow\Downarrow\rangle$ to $|\downarrow\Uparrow\rangle$ during step {13} . We have improved on this scheme for these D^+ studies by adding a readout laser on line 5, so that both the $|\downarrow\Uparrow\rangle$ and $|\uparrow\Uparrow\rangle$ populations are read out simultaneously, doubling the signal and eliminating the 30 ms transients seen in Fig. 2B. Also, since the electron state of individual donors is arbitrary during the readout in our new scheme, π pulses at all three NMR frequencies are applied at step {12} to flip all ^{31}P nuclear spins.

The fast (~5 ms) buildup transient in Fig. 2C is the time needed to convert D^0 to D^0X under our excitation conditions (the D^0X Auger decay time is 272 ns (*18*)), and the ~

25 ms decay time is the time taken to recapture e^- onto D^+, giving a $D^0 \rightarrow D^0X \rightarrow D^+ \rightarrow D^0$ cycle time of ~30 ms, in agreement with the transients seen in Fig. 2B. This time for the donor measurement cycle was combined with the decay seen in Fig. 2D to arrive at the estimate of at least 250 D^0X cycles before the nuclear polarization decayed to 1/e.

Maximum magnitude detection

When using a simple Hahn echo pulse sequence, a problem known as phase noise often appears at long delay times. This occurs because either the RF frequency or the B_0 field varies between the first half and the second half of the Hahn echo sequence, so that the phase of the nuclear spin echo becomes uncorrelated with the RF phase at readout. In standard magnetic resonance experiments this can be easily remedied, since both the in-phase and quadrature echo signals (X and Y) can be captured simultaneously, allowing an echo magnitude to be calculated (*31*). Our projective readout can only measure one particular phase of the echo for each shot, precluding this approach. However, even with a completely random phase, the absolute value of the projective readout will be within 98% of the maximum possible echo signal for 10% of the readouts. We implement this by taking 40 measurements at each delay and averaging the 4 largest absolute values to obtain our echo strength. This method will fail at long delays once the signal approaches the noise floor, but the observed single exponential decay shows that we have not reached this noise limit.

Supplementary Text

Possible polarization and coherence decay mechanisms for D^0 at low T

We have already remarked on the near agreement between the observed D^0 (*9*) and D^+ Hahn echo T_2 times, which could have suggested a common mechanism given that the same sample material was used, a possibility which is excluded by the further observation that XY-16 decoupling extends T_2 by a factor of 400 for D^+ but only 4.4 for D^0. Our D^+ results are well-accounted for by a combination of B_0 inhomogeneity and spectral diffusion due to the spins of the remaining ^{29}Si (*13*), and we now reexamine the possible mechanisms limiting the D^0 results both for the p-type Avogadro material (*9*) as well as the n-type material used in the original optical-NMR study (*16*), which has the same ^{28}Si enrichment as the Avogadro samples but ~1000 times more ^{31}P.

The spin Hamiltonian for an isolated $^{31}P^0$ in a magnetic field B_0 along the **Z** axis can be written:

$$H = g_e\mu_B B S_z - g_n\mu_n B I_z + a\boldsymbol{S}\cdot\boldsymbol{I} \qquad (1)$$

where $\boldsymbol{S}$ and $\boldsymbol{I}$ are the electron and ^{31}P nuclear spins, respectively and a is the hyperfine constant (the Hamiltonian for $^{31}P^+$ has only the central term). In frequency units, $g_e\mu_B/h \cong 2.79715$ MHz/G, $g_n\mu_n/h \cong 1.723$ kHz/G, and $a/h = A \cong 117.53$ MHz (*16*). The hyperfine coupling present for D^0 allowed nuclear coherence measurements (*9*, *16*) to be done at a field (~845.3 G) where $\partial RF\uparrow/\partial B_0 = \partial RF\downarrow/\partial B_0 = 0$, also referred to as a 'clock transition'. This was done to relax the requirement for B_0 homogeneity, given our relatively low homogeneity electromagnet (*16*). That this was successful can be seen by the fact that improving the B_0 homogeneity by adding ring shims to the magnet, which improved the Ramsey fringe T_2^* for D^+ from 0.8 ms to 4.2 ms, had no effect on T_2^* for D^0, which was 38 ms before and after shimming, as seen in Fig. S3. Operating at a clock

transition additionally makes the frequency very insensitive to small fluctuations in B_0, greatly suppressing decoherence due to spectral diffusion processes (*32*). We therefore consider other mechanisms, which do not involve B_0 noise, as possible sources for the coherence signal decay in the D^0 case.

We have already mentioned that in the early stages of this study of D^+ we observed decay in the D^0 population in the dark after photoneutralization resulting from donor-acceptor-pair recombination (*15*). This process caused a Z-polarized D^0 T_1 signal at 1.3 K to decay to 1/e in ~1000 s, even though the actual T_1 is expected to be much longer. This neutral donor population decay makes a small contribution to all the decay times reported previously (*9*) for the D^0 system.

Given that for D^0 the use of the clock transition should suppress the effects of noise and inhomogeneity in B_0, we believe that the major source of decoherence and inhomogeneous broadening for the D^0 nuclear spins in our experiments arise from modulations of the hyperfine coupling A. At our B_0 and higher, $\partial RF\uparrow/\partial A \cong \partial RF\downarrow/\partial A \cong 0.5$, and with $A \cong 117$ MHz even very small fractional changes or noise in A can be responsible for decoherence. The hyperfine constant can be affected by electric field (*33*,*34*) or strain (*35*), and it is interesting to note that even changing the sample environment from 1.3 K and near-zero pressure to 4.2 K and atmospheric pressure changes A for ^{31}P by 3.1 kHz (*16*), a very large change in frequency on the scale of the coherence times observed for neutral ^{31}P.

The modulation of A by static inhomogeneous fields in the sample arising from chemical impurities such as the ^{31}P itself, or electrically inactive impurities such as C and O, or even from the remaining ^{29}Si and ^{30}Si (*36*) can explain the D^0 T_2* of 38 ms for the present sample, which at first seemed surprisingly short given that the measurements were done at a clock transition. This is supported by the observation that a shorter T_2* of 16.4 ms was observed for the n-type sample (*16*), and that the ratio of the T_2*'s, 2.3, is almost identical to the ratio of 2.2 between the inhomogeneously broadened bound exciton spectral linewidths in the two samples, with a full width at half maximum of 7.6 x 10^{-4} cm^{-1} for the Avogadro sample and 1.7 x 10^{-3} cm^{-1} for the n-type sample.

In considering the coherence times previously reported for D^0 in the same material, we begin by noting that the temperature dependence of the XY-16 decoupled T_2 times shown in Fig. 3 of (*9*) can be accurately explained by the sum of a temperature dependent decay rate related to T_{1e} (*10*) and a temperature independent rate of ~1/200 s^{-1}. The T_{1e} process is easily understood, causing a direct flip of the electron of the central coherent spin, which cannot be recovered by dynamic decoupling given the large frequency difference between RF↑ and RF↓. This process dominates at 4.2 K, limiting the T_2 of 41 s to two times T_{1e}, which was measured under the same conditions to be 21 s. The limiting low temperature T_2 of ~ 200 s may result from several contributions, one of which is likely to be direct electron flip-flops between coherent 'central' donors which have electron spin down with donors having electron spin up, which would again destroy the coherence almost instantly, and not be recoverable by dynamic decoupling. This process would be suppressed by the degree of electron polarization, but we have determined that under the conditions used in (*9*), at the beginning of the measurement time ~5% of the donors had incorrectly polarized electrons, and ~5% of the donors were ionized. This is a dipolar process which should scale as the donor concentration, and it is interesting to note that the 230 ms T_2 observed for the n-type sample was approximately 1000 times shorter

than the 192 s observed for the Avogadro sample, in reasonable agreement with the ~1000 times difference in ^{31}P concentration.

There must also be a contribution to the low temperature T_2 which can be lengthened by the XY-16 decoupling, which was able to extend T_2 from 44 s to 192 s. One candidate is spectral diffusion due to indirect donor electron flip-flops, which might not be completely suppressed by operating at the clock transition. Another could be modulation of A by electric field noise, as the photoneutralized donors and acceptors slowly ionize in the dark by donor-acceptor- pair recombination. Estimating the size of this effect is difficult, since measurements of the hyperfine Stark shift for Sb in Si give a value -3.7x10^{-3} μm^2/V^2 (*33*), considerably smaller than the -2 x10^{-2} μm^2/V^2 calculated for ^{31}P (*33*,*34*). Taking these two values, the ionization of an impurity located 1 μm from a coherent donor, as is roughly appropriate for the impurity concentrations in the p-type Avogadro sample, would produce a hyperfine shift of the NMR frequency by ~19 mHz or ~3.6 mHz, which could contribute significantly to the 44 s Hahn echo T_2 and still be ameliorated by the XY-16 dynamical decoupling. The hyperfine Stark effect due to the static electric fields from ionized impurities could also contribute to the observed T_2*, but even assuming that 10% of the donors are ionized immediately after the hyperpolarization process, the resulting electric field distribution (*37*) would produce a frequency broadening of only ~1 Hz or ~0.2 Hz, making a very small contribution to the 38 ms T_2*.

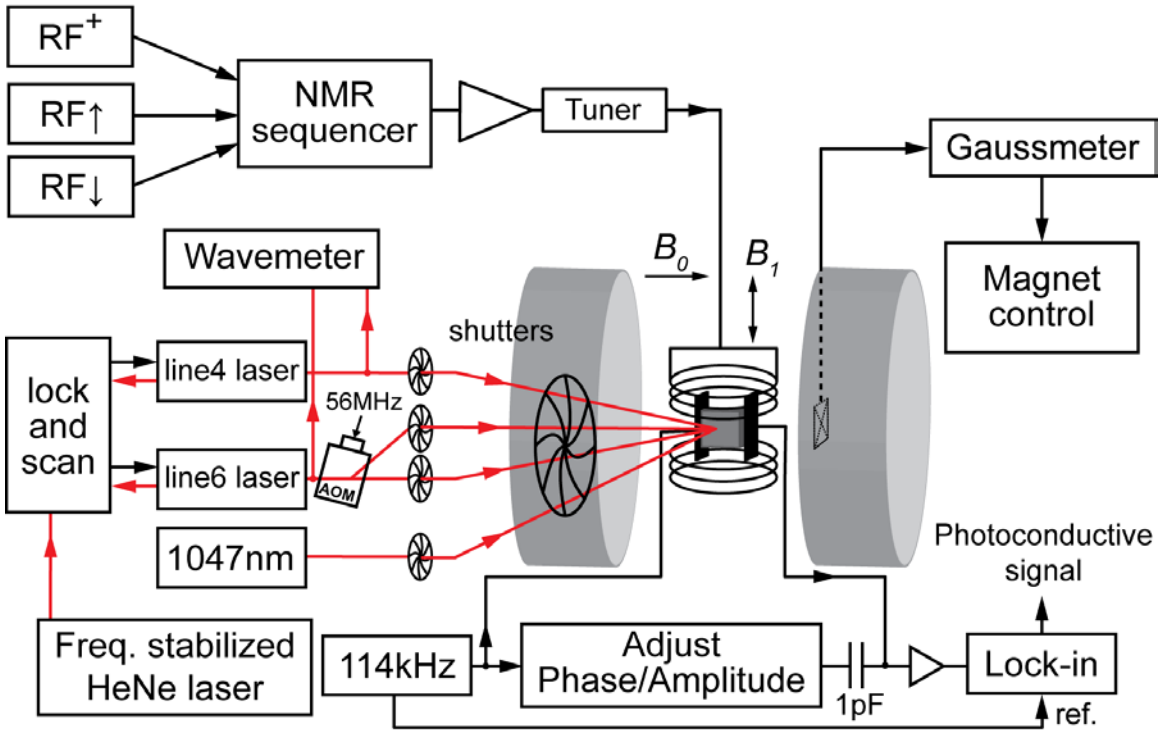

Fig. S1.

A block diagram of the experimental apparatus. The electromagnet system used for the constant temperature cryogenic experiments is shown.

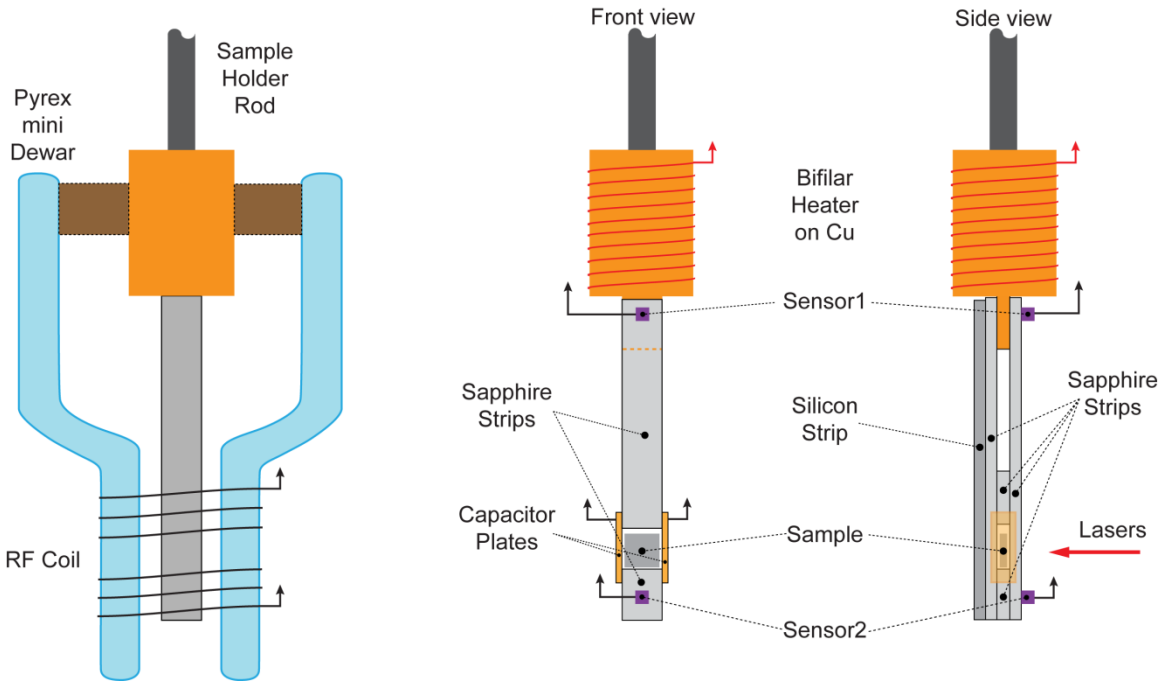

Fig. S2

The sample holder and mini-dewar assembly used for the temperature ramp experiments.

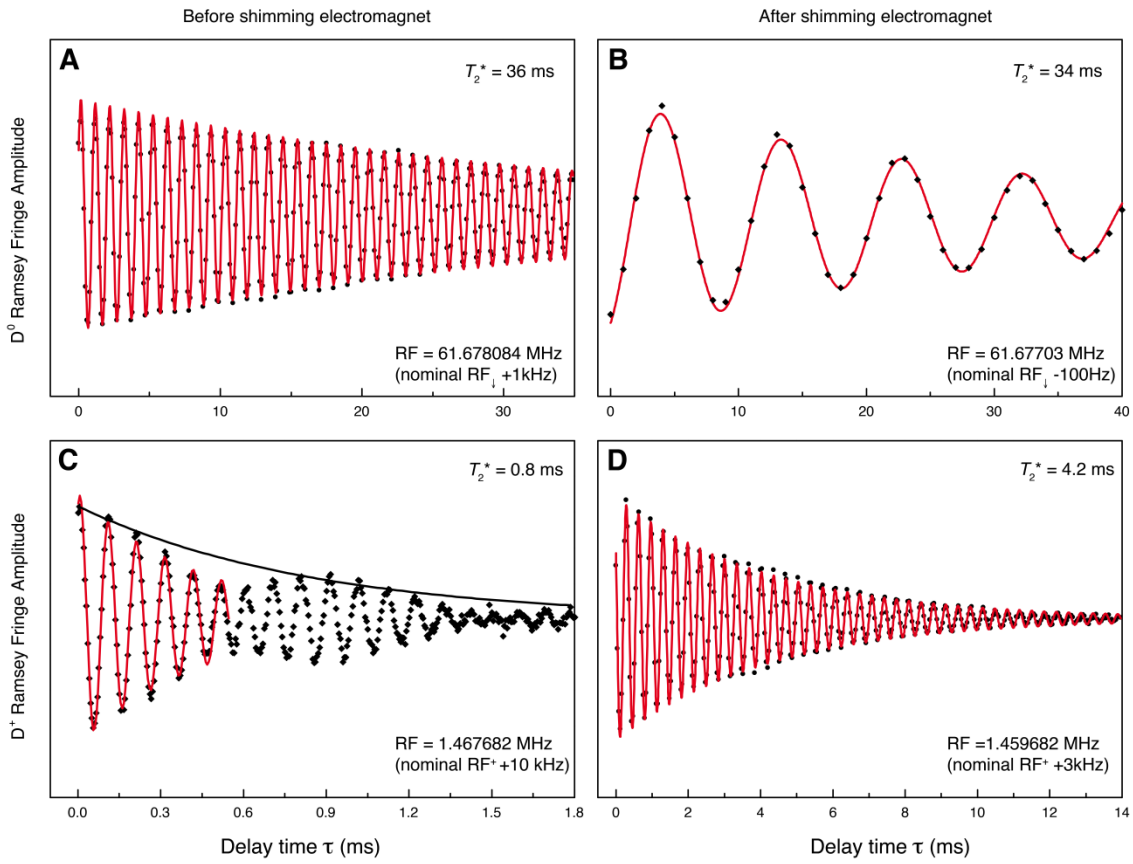

Fig. S3

Ramsey fringe scans for D^0 on the RF↓ transition and for D^+ are shown in A to D before and after improving the B_0 homogeneity by placing circular ring shims on the electromagnet. The fits to the data are a sinusoidal function, which gives the fringe frequency, multiplied by an exponential decay, which gives T_2*. The applied RF frequency in each case was the nominal expected resonance frequency plus or minus a shift which should equal the observed fringe frequency. The exact resonance frequency under the experimental conditions of the scan is the given by the applied RF frequency minus or plus the observed fringe frequency. The increase in T_2* from improving the B_0 homogeneity by shimming is large for D^+, but absent for D^0, since the D^0 measurement takes place at a clock transition.

References and Notes

1. D. Deutsch, Quantum theory, the Church-Turing principle and the universal quantum computer. *Proc. R. Soc. London Ser. A* **400**, 97–117 (1985). doi:10.1098/rspa.1985.0070

2. T. D. Ladd, F. Jelezko, R. Laflamme, Y. Nakamura, C. Monroe, J. L. O'Brien, Quantum computers. *Nature* **464**, 45–53 (2010). doi:10.1038/nature08812 Medline

3. S. Wiesner, Conjugate coding. *ACM SIGACT News* **15**, 78–88 (1983). doi:10.1145/1008908.1008920

4. F. Pastawski, N. Y. Yao, L. Jiang, M. D. Lukin, J. I. Cirac, Unforgeable noise-tolerant quantum tokens. *Proc. Natl. Acad. Sci. U.S.A.* **109**, 16079–16082 (2012). doi:10.1073/pnas.1203552109

5. P. C. Maurer, G. Kucsko, C. Latta, L. Jiang, N. Y. Yao, S. D. Bennett, F. Pastawski, D. Hunger, N. Chisholm, M. Markham, D. J. Twitchen, J. I. Cirac, M. D. Lukin, Room-temperature quantum bit memory exceeding one second. *Science* **336**, 1283–1286 (2012). doi:10.1126/science.1220513 Medline

6. B. E. Kane, A silicon-based nuclear spin quantum computer. *Nature* **393**, 133–137 (1998). doi:10.1038/30156

7. J. J. Morton, D. R. McCamey, M. A. Eriksson, S. A. Lyon, Embracing the quantum limit in silicon computing. *Nature* **479**, 345–353 (2011). doi:10.1038/nature10681 Medline

8. D. D. Awschalom, L. C. Bassett, A. S. Dzurak, E. L. Hu, J. R. Petta, Quantum spintronics: Engineering and manipulating atom-like spins in semiconductors. *Science* **339**, 1174–1179 (2013). doi:10.1126/science.1231364 Medline

9. M. Steger, K. Saeedi, M. L. Thewalt, J. J. Morton, H. Riemann, N. V. Abrosimov, P. Becker, H. J. Pohl, Quantum information storage for over 180 s using donor spins in a ^{28}Si "semiconductor vacuum". *Science* **336**, 1280–1283 (2012). doi:10.1126/science.1217635 Medline

10. G. Feher, E. A. Gere, Electron spin resonance experiments on donors in silicon. II. Electron spin relaxation effects. *Phys. Rev.* **114**, 1245–1256 (1959). doi:10.1103/PhysRev.114.1245

11. L. Dreher, F. Hoehne, M. Stutzmann, M. S. Brandt, Nuclear spins of ionized phosphorus donors in silicon. *Phys. Rev. Lett.* **108**, 027602 (2012). doi:10.1103/PhysRevLett.108.027602 Medline

12. J. J. Pla, K. Y. Tan, J. P. Dehollain, W. H. Lim, J. J. Morton, F. A. Zwanenburg, D. N. Jamieson, A. S. Dzurak, A. Morello, High-fidelity readout and control of a nuclear spin qubit in silicon. *Nature* **496**, 334–338 (2013). doi:10.1038/nature12011 Medline

13. W. M. Witzel, M. S. Carroll, Ł. Cywiński, S. Das Sarma, Quantum decoherence of the central spin in a sparse system of dipolar coupled spins. *Phys. Rev. B* **86**, 035452 (2012). doi:10.1103/PhysRevB.86.035452

14. Supplementary materials are available on *Science* Online.

15. P. Dirksen, A. Henstra, W. Th. Wenckebach, An electron spin-echo study of donor-acceptor recombination. *J. Phys. Condens. Matter* **1**, 7085–7092 (1989). doi:10.1088/0953-8984/1/39/020

16. M. Steger, T. Sekiguchi, A. Yang, K. Saeedi, M. E. Hayden, M. L. W. Thewalt, K. M. Itoh, H. Riemann, N. V. Abrosimov, P. Becker, H.-J. Pohl, Optically-detected NMR of optically-hyperpolarized ^{31}P neutral donors in ^{28}Si. *J. Appl. Phys.* **109**, 102411 (2011). doi:10.1063/1.3577614

17. W. Schmid, Auger lifetimes for excitons bound to neutral donors and acceptors in Si. *Phys. Status Solidi* **84**, 529–540 (1977) (b). doi:10.1002/pssb.2220840216

18. D. R. McCamey, J. Van Tol, G. W. Morley, C. Boehme, Electronic spin storage in an electrically readable nuclear spin memory with a lifetime >100 seconds. *Science* **330**, 1652–1656 (2010). doi:10.1126/science.1197931 Medline

19. T. Gullion, D. B. Baker, M. S. Conradi, New, compensated Carr-Purcell sequences. *J. Magn. Reson.* **89**, 479–484 (1990).

20. W. Burger, K. Lassmann, Energy-resolved measurements of the phonon-ionization of $D^-$and A^+ centers in silicon with superconducting-Al tunnel junctions. *Phys. Rev. Lett.* **53**, 2035–2037 (1984). doi:10.1103/PhysRevLett.53.2035

21. T. D. Ladd, D. Maryenko, Y. Yamamoto, E. Abe, K. M. Itoh, Coherence time of decoupled nuclear spins in silicon. *Phys. Rev. B* **71**, 014401 (2005). doi:10.1103/PhysRevB.71.014401

22. R. Jozsa, Fidelity for mixed quantum states. *J. Mod. Opt.* **41**, 2315–2323 (1994). doi:10.1080/09500349414552171

23. J. J. L. Morton, A. M. Tyryshkin, R. M. Brown, S. Shankar, B. W. Lovett, A. Ardavan, T. Schenkel, E. E. Haller, J. W. Ager, S. A. Lyon, Solid-state quantum memory using the ^{31}P nuclear spin. *Nature* **455**, 1085–1088 (2008). doi:10.1038/nature07295

24. M. Steger, A. Yang, M. Thewalt, M. Cardona, H. Riemann, N. Abrosimov, M. Churbanov, A. Gusev, A. Bulanov, I. Kovalev, A. Kaliteevskii, O. Godisov, P. Becker, H.-J. Pohl, E. Haller, J. Ager, High-resolution absorption spectroscopy of the deep impurities S and Se in ^{28}Si revealing the ^{77}Se hyperfine splitting. *Phys. Rev. B* **80**, 115204 (2009). doi:10.1103/PhysRevB.80.115204

25. W. F. Koehl, B. B. Buckley, F. J. Heremans, G. Calusine, D. D. Awschalom, Room temperature coherent control of defect spin qubits in silicon carbide. *Nature* **479**, 84–87 (2011). doi:10.1038/nature10562 Medline

26. P. Becker, H.-J. Pohl, H. Riemann, N. V. Abrosimov, Enrichment of silicon for a better kilogram. *Phys. Status Solidi* **207**, 49–66 (2010) (a). doi:10.1002/pssa.200925148

27. T. Sekiguchi, M. Steger, K. Saeedi, M. L. Thewalt, H. Riemann, N. V. Abrosimov, N. Nötzel, Hyperfine structure and nuclear hyperpolarization observed in the bound exciton luminescence of Bi donors in natural Si. *Phys. Rev. Lett.* **104**, 137402 (2010). doi:10.1103/PhysRevLett.104.137402 Medline

28. L. Viola, S. Lloyd, Dynamical suppression of decoherence in two-state quantum systems. *Phys. Rev. A* **58**, 2733–2744 (1998). doi:10.1103/PhysRevA.58.2733

29. Z.-H. Wang, W. Zhang, A. M. Tyryshkin, S. A. Lyon, J. W. Ager, E. E. Haller, V. V. Dobrovitski, Effect of pulse error accumulation on dynamical decoupling of the electron spins of phosphorus donors in silicon. *Phys. Rev. B* **85**, 085206 (2012). doi:10.1103/PhysRevB.85.085206

30. S. Wimperis, Broadband, narrowband, and passband composite pulses for use in advanced NMR experiments. *J. Magn. Reson. A* **109**, 221–231 (1994). doi:10.1006/jmra.1994.1159

31. A. M. Tyryshkin, S. Tojo, J. J. Morton, H. Riemann, N. V. Abrosimov, P. Becker, H. J. Pohl, T. Schenkel, M. L. Thewalt, K. M. Itoh, S. A. Lyon, Electron spin coherence exceeding seconds in high-purity silicon. *Nat. Mater.* **11**, 143–147 (2011). doi:10.1038/nmat3182 Medline

32. G. Wolfowicz, A. M. Tyryshkin, R. E. George, H. Riemann, N. V. Abrosimov, P. Becker, H. J. Pohl, M. L. Thewalt, S. A. Lyon, J. J. Morton, Atomic clock transitions in silicon-based spin qubits. *Nat. Nanotechnol.* **8**, 561–564 (2013). doi:10.1038/nnano.2013.117 Medline

33. F. R. Bradbury, A. M. Tyryshkin, G. Sabouret, J. Bokor, T. Schenkel, S. A. Lyon, Stark tuning of donor electron spins in silicon. *Phys. Rev. Lett.* **97**, 176404 (2006). doi:10.1103/PhysRevLett.97.176404 Medline

34. M. Friesen, Theory of the Stark effect for P donors in Si. *Phys. Rev. Lett.* **94**, 186403 (2005). doi:10.1103/PhysRevLett.94.186403 Medline

35. L. Dreher, T. A. Hilker, A. Brandlmaier, S. T. Goennenwein, H. Huebl, M. Stutzmann, M. S. Brandt, Electroelastic hyperfine tuning of phosphorus donors in silicon. *Phys. Rev. Lett.* **106**, 037601 (2011). doi:10.1103/PhysRevLett.106.037601 Medline

36. D. Karaiskaj, G. Kirczenow, M. L. Thewalt, R. Buczko, M. Cardona, Origin of the residual acceptor ground-state splitting in silicon. *Phys. Rev. Lett.* **90**, 016404 (2003). doi:10.1103/PhysRevLett.90.016404 Medline

37. D. M. Larsen, Inhomogeneous broadening of the Lyman-series absorption of simple hydrogenic donors. *Phys. Rev. B* **13**, 1681–1691 (1976). doi:10.1103/PhysRevB.13.1681